# Biophysical Studies of the Effect of MreB Mutants on Cell Stiffness in *Escherischa Coli*

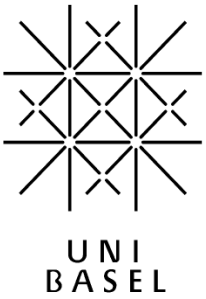



Master Thesis in Nanosciences

**Benjamin Banusch (B.Sc.)**

benjamin.banusch@stud.unibas.ch

November 30th, 2013

Supervisor:
Prof. Joshua Shaevitz
Department of Physics and Lewis-Sigler Institute for Integrated Genomics
Princeton University, USA

Home Advisor:
Prof. Thomas Pfohl
Department of Chemistry, Institute for Physical Chemistry
University of Basel, CH

**Abstract**

As part of the fundamental question of how bacterial shape can be obtained and what proteins are involved, bending experiments on *E.coli* bacteria with mutations in mreB were conducted to provide answers to open questions in terms of the function of MreB in peptidoglycan (PG) biosyntheses. Coloborators at Stanford [59] discovered MreB mutants which differ in cell width and investigations were conducted to measure if the mechanical properties of the cell wall and MreB bundles were different in these mutants. Using a bending cell assay consisting of optical tweezers and microfluidic channels, we repeat former experiments by Siuyan Wang [3] to prove the influennce of MreB bundles on the mechanical property of the cell. Resulting values for the flexural reigidity (EI), cell width in M9 media and elastic moduli could be provided and it was shown that MreB contributes 8-20% to the overall cell stiffness, depending on differences in MreB. Also, precice cell width measurements, using the basics for a 3D fluorescence microscopy technique [19], were measured and correlated with existing flexural rigidities of MreB mutants. Results show a clear cell radius dependency of the bending stiffness with $EI \propto R^3$ and provide evidence for a single MreB function. Our results indicate that the function of PG synthesis colocalized MreB bundles include the localization of new cell wall material but no insertion of material or the constuction of the cell wall itself. Therefore, a big step in understanding the bacterial shape conformation and cell wall syntheses was made and a new theory of the function of MreB filaments was provided.

# Contents

## Abbreviations

| | | |
|---|---|---|
| LB | = | lysogeny broth |
| PEI | = | PolyEthylenImine |
| OD | = | Optical Density |
| BSA | = | Bovine serum albumin |
| PG | = | PeptidoGlycan |
| Cpt | = | Cytoskeleton Polimerization inhibiting Toxin |
| A22 | = | PeptidoGlycan |
| ADP | = | Adenosindiphosphat |
| ATP | = | Adenosintriphosphat |
| PBP2 | = | Penicilin Binding Protein 2 |
| A22 | = | 3,4-Dichlorobenzyl)-isothiourea |

# 1 Biological and Physical Background

## 1.1 MreB, the Actin equivalent

MreB, the actin homolog in bacteria, is part of the bacterial cytoskeleton and can be found in most non sperical bacteria, gram-positive as well as gram-negative. MreB monomers are small proteins with a size of about 36 kDa. The amount of MreB monomers varies between species and exists on the order of 2000 to 40.000 in a single cell [3]. MreB is encoded in the chromosome and all characterized homologs can polymerize into filaments [60,36]. Well-known for its helical shape, recent studies with electron chromatogrphy revealed that the observed long helical filaments of MreB are just artifacts, induced by YFP tagged MreB [35]. Instead MreB forms short protofilaments which vary in size within a species. Typical lengths are between a couple hundred nanometers to micrometers [45]. The polymerization is ATP dependent [van Ent 2001] and can be inhibited by different Ctp (Cytoskeleton Polimerization inhibiting Toxin) such as YgfX or A22 [1, 2]. By using fluorescence microscopy techniques with for example GFP-MreB fusions , the localization of MreB could be determined all around the cell at the inner site of the plasma membrane. The binding is associated with a membrane insertion loop in TmMreB and a helix structure in ECMreB [13] (Figure 2). In the actin superfamily, MreB was one of the first examples of membrane binding filaments. Different studies show an additional interaction with the inner membrane protein RodZ [10] (Figure 1). Both RodZ and MreB are well known for their contribution to cell shape determination. Deletion of mreB and rodZ lead to lemon-shaped or spherical bacteria [10,48,51] and studies indicate the MreB- RodZ interaction is important for bacteria to maintain cell shape [5]. MreB colocalizes with the peptidpglycan biosyntheses and the characteristic shape determination is most likely mediated by the peptidoglycan architecture .Recent studies show that a left handed chirality of the MreB protofilament leads to a right handed chiral order of the peptidoglycan. Therefore, MreB responsible for the guidance for local insertion of

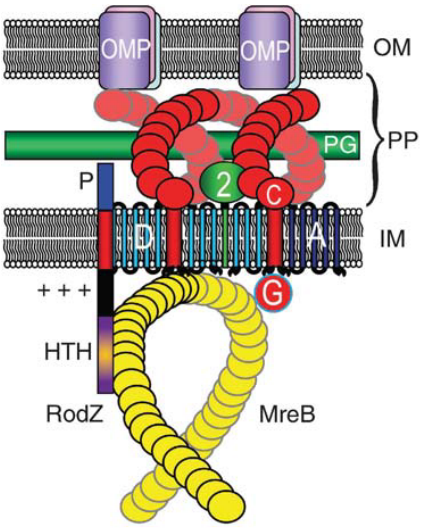


Figure 1: Location and orientation of MreB polymer at the inside of the cell membrane [31]. Additional illustrates proteins are MreD (D), RodA (A), MreC with PBP2 etc. as well as the Outer membrane protein (OMP).

material into the peptidoglycan and thereby coordinates cell wall architecture [18]. It is still unclear if MreB is somehow coupled to the peptidoglycan or if it indirectly supports peptidoglycan syntheses. Studies by Siuyan Wang and this thesis show MreB contributes a significant amount to cell stiffness [3]. An explanation could be based on the assumption that MreB is connected to the cell wall peptidoglycan, but current theories include just a tansient attachement to the cell wall during peptidoglycan syntheses and assumes that MreB is a rigid polymer. However, the last decades revealed additional property of MreB and how it influences cell shape. One important properties is its motion. Driven by cell wall syntheses, MreB moves around the cell in an helical path with a speed of around 80nm per minute [34]. Besides giving bacterial cells its characteristic shape [4], MreB is also associated with their cell devision [42,49,50], chromosome segregation [47] and cell wall morphogenisis [48].

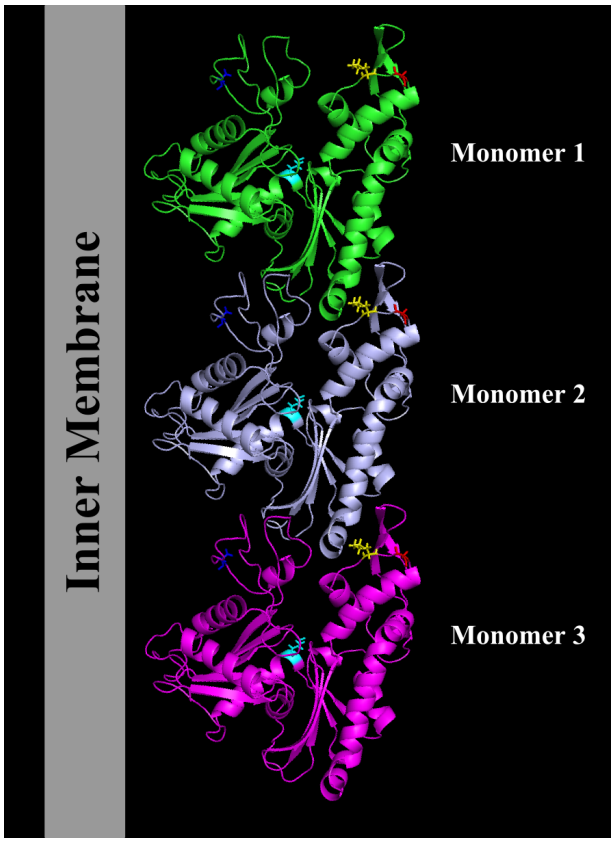


Figure 2: Homology model of MreB in *E.coli* [56] with approximate monomer-monomer interaction and orientation to plasma membrane. Three different MreB monomers are illustrated. The colored amino acids matching the residues A53 (blue), G207 (red), L209 (yellow) and L322 (cyan).

### 1.1.1 The Drug A22: Inhibitor of MreB Polymerization

The relativly new drug A22 is a member of the 'Cytoskeleton Polimerization inhibiting Toxin'-family [1]. The chemical name of A22 is 3,4-Dichlorobenzyl)-isothiourea (Figure3) and it is well known for its property, to inhibit polymerization of the actin homolog MreB. Also, A22 is causing defects in bacteria concerning cell morphology and chromosome segregation. However, A22 is mainly used to cause depolymerization of MreB. Recent publications show, that A22 binds at least with a micromolar affinity to the nucleotide binding pocket of MreB monomer / polymers. Therby it mimics ADP and prevents ATP (Adenosine triphosphate) from binding to ATP-binding pocket inhibits MreB to polymerize into short filaments [2,7]. Polymerization and depolymerization of MreB filaments is an ongoing process and by blocking polymerization, MreB depolimerizes within several minutes [3]. Because of this unique characteristic A22 is commonly used to study the behavior of bacteria with and without MreB bundles.

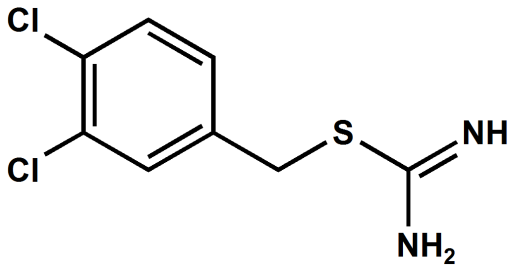


Figure 3: S-(3,4-Dichlorobenzyl)isothiourea

# 2 Materials and Methods

## 2.1 Chemicals, Materials and experimental set up

| **Material** | **Company and Model** | **Properties** |
|---|---|---|
| Microscope Cover Glass | Fisherbrand 12-545-C 22X40-1 | Thickness and Size: 0.13-0.17mm;40x22mm |
| Microscope Micro Slides | Gold Seal Cat No 3010 | Thickness and Size: 0.96-1.06mm;75x25mm |
| 0.1%Poly-L-lysine solution | Sigma-Aldrich CAS Number:25988-63-0 | Molecular weight range: 70 - 150 kDa |
| PolySterene beads Dragon Green (480,520) | Bang- Baboratories Catalog Code FS03F | Mean diameter: 0.52m |
| PolySterene beads | Bang- Baboratories Catalog Code PS03N | Mean diameter: 0.52m |
| FM 4-64FX | Life Technologies Product code: F34653 | WGA fluorescence dye Location: Plasma membrane |
| Double Sided tape 3M | Scotch model number: MMM136 | Size 12.7mm x 22.8m |
| Microscope | Nikon eclipse TE2000-S | Inverted with filter sets |
| Position Sensitive Detector (PSD) | Newport model 2931 | 9x9 mm, 8-32 M4 thread 2m resolution +-25m accuracy |
| Camera | Andor $iXon^{-}+$ | with cooling system |

Table 1: Used Chemicals and Materials for the bending protocol and width measurements

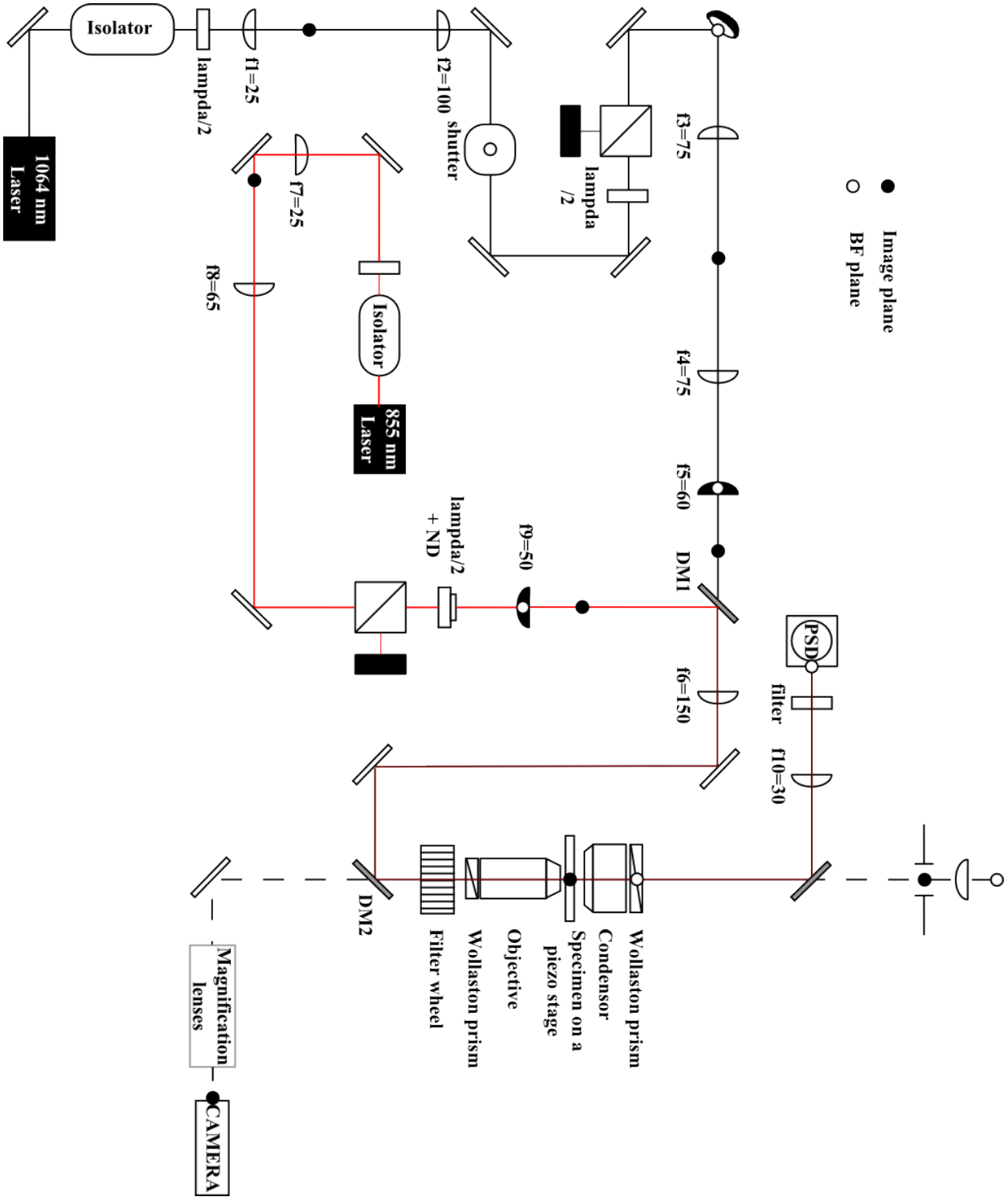


Figure 4: Experimental set up with optical circuit

## 2.2 Bacterial Strains and Mutations

To verify if differences in bacterial cell stiffness occur through variation within the genotype of the model bacterium *E.coli*, the wild type B-strain and selected mreB mutants were chosen. Collaborators at Stanford University, Russel Monde and K.C.Huang, identified a series of mreB mutants which differ in relative fitness and cell width. The relative fitness can be described as the average growth rate on a head to head competition between selected strains. An identified mutation in mreB-A53T showed an increase in width and a fitness advantage at the same time. A prediction of a positive correlation between cell width and fitness was made and open questions in terms of differences in cell wall composition, construction and MreB influence lead to the thesis, that the determination of bacterial stiffness could help, proof this assumption. Prior experiments showed that the bacterial stiffness can be determined [3] with a bending cell assay using optical tweezers and microfluidic channels. The mreB-A53T mutant was selected through subculturing and different experiments indicate an influence on polymer stability [55]. This particular mutation most likely destabilizes the MreB polymer, which effects the MreB structure and polymerization [22]. Through suppressor screening of A22 sensitivity, additional mutations were found by Russel Monde [59] which seem to restabilize the MreB polymer and lead to a normalized cell width, in comparison to the A53T-mutant. An additional second point mutation in mreB-L322Q, which is located in or close to the ATP binding pocket show an normalization of overall cell width. A similar effect could be observed with two additional suppressor mutations in mreB-G207C and mreB-L209R. Both are located in the monomer-monomer interaction domain and seem to stabilize the protofilaments as well. Figure 5 shows an unpublished homology model of MreB in *E.coli* [56] with the locations of the point mutations in A53T, G207C, L209C and L322Q. In this orientation of the monomer, the inner membrane would be on the left side. Characteristics and names of used bacterial strains are shown in (Appendix) Table 4.

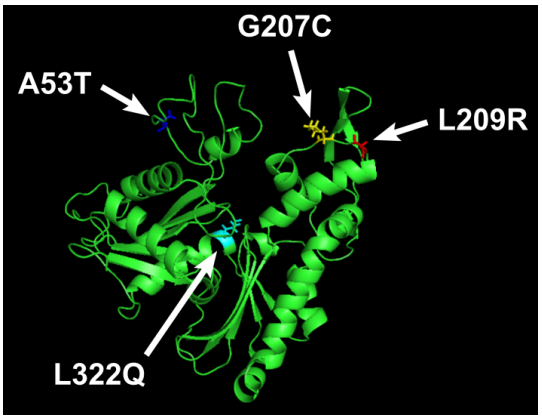


Figure 5: Homology model of MreB in *E.coli* [56] with labeled residues numbers for point mutations in A53T, G207C, L209R and L322Q.

## 2.3 Bending Assay

For all bending experiments and to determine the flexural rigidity and bending stiffness of all *E.coli* strains, a modified bending protocol was used. The original bending assay was developed and implemented by PhD Siuyen Wang and Prof. Joshua Shaevitz [3]. Their protocol consists of a different media condition and corresponding time scales. However, for practical reasons and to improve the existing protocol in terms of bead- cell attachment and experimental window, we decided to modify the original bending assay.

### 2.3.1 Original Sample Preparation

The original protocol was developed by PhD Siyuen Wang and contained the following steps. The selected *E.coli* strains were grown over night in LB at 37° to gain a high concentration of cells. Furthermore the cells were diluted 1:1000 in LB and grown to exponential phase (OD=0.2-0.4). Afterward, cells were grown with 50$\mu$l Cephalexin for 15min at 37°C to induce filamentous growth and concentrated five-fold by centrifugation. Microfluidic channels were made with two stripes of double sided tape, flooded with 1% PEI diluted in water and incubated for 5min. The PEI coated channels were washed with water and 50$\mu$ of cells were injected for immobilization purposes. Cells were incubated for 3min at room temperature and washed 3 times with LB media. Then, the channels were incubated for 30-60min at 37° before applying the bending protocol. Polysterene beads were coated with 0.1% poly-Lysine solution by incubation for 30min and washed 3 times in water. For A22 measurements, a 50$\mu$l/ml A22 working solution was made in LB.

### 2.3.2 Reasons for Modification

Multiple aspects of the former developed protocol [3] indicated a necessary improvement for the bending experiments. One concerning issue rely on the bead-cell attachment of the protocol. Poly-L-Lysine coated polysterene beads show an decrease attachment to the immobilized cells, caused by the used LB medium. The LB medium was blocking the poly-Lysine and prevented an appropriate bead cell attachment. The large applied forces of the optical trap show that the coated polysterene beads got 'unsticky' over time, and therefore better media condition had to be found. M9 Glucose minimal media was one possible solution and showed excellent physical properties for our purposes. But also, the increased bead cell attachment lead to an additional increase in cell- surface attachment. During measurements, cells attached spontaneously to the surface and did not allow the conduction of measurements. Therefore, 0.2% BSA was added to all M9 media to decrease cell-surface attachment of the free hanging tip of immobilized cells. The mixture of 0.2%BSA and M9 Glucose minimal medium was the perfect

choice for later measurements and solved the existing problems. An additional aspect of the new media was the increased growth time which lead to a longer experimental window at the microscope and improved the measured cell per day ratio. But this was a disadvantage at the same time. Longer growth rates prolong the time for a single experiment, and therefore another solution had to be found. This solution was based on a media change before the immobilization of cells to the surface. The switch of media conditions combines the advantages in terms of growth rate (Figure 6) and bead-cell attachment and allowed a higher throughput on a single day basis.

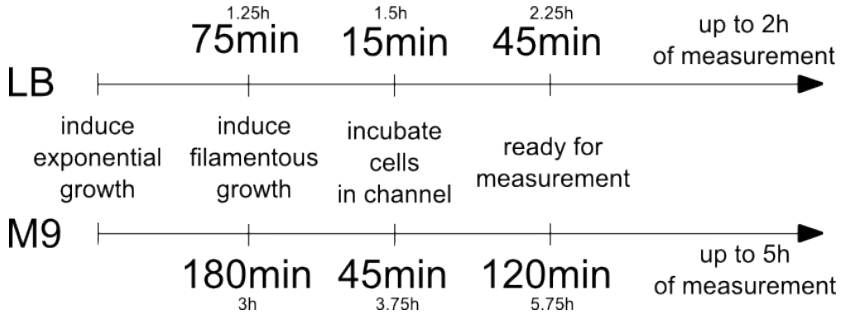


Figure 6: Time scales of different growth media condition for the sample preparation of the bending protocol. A switch in media condition was induced after filamentous growth and before immobilization of cells in the microfluidic channel.

### 2.3.3 Modified Sample Preparation

The modified protocol was used as a preparation for all bending measurements on all *E.coli* strains. First, a prior selected *E.coli* strain was grown 8 to 16 hours in LB medium at 37° to get an high concentration of cells. The liquid culture was then diluted in LB medium 1:1000 and again grown for 60-75min at 37°C to exponential phase and to reach a final cell concentration of OD= 0.1-0.15. A concentration of 50$\mu$g/ml Cephalexin was added to induce filamentous growth and again incubated for 30min at 37°. For this protocol, a simple microfluidic device was made, consisting of two cover slides of different size (Fisherbrand and Gold Seal), connected via two layers of double- taped tape (Scotch) to create a channel with an inlet and outlet. The channel size was less then a centimeter. A medium switch was initialized from LB to M9 medium by centrifugation. For the immobilization of *E.coli* cells, the channel was flooded with 1% PEI solution for 5min and washed with 200$\mu$l water. 50$\mu$l of cells were injected into the channel for 3min, washed afterward 3 times with 0.2% BSA M9 Glucose minimal media and incubated for 60-90min at 37°. The prepared samples were then used for bending measurements. For detection purposes and later calibrations,

0.52$\mu$m thick polysterene beads (Bang Lab.) were coated with 0.1% poly-Lysine solution (Sigma) for 30min and washed 3 times with water. For A22 measurements, 10mg/ml A22 in Methanol was diluted 1000 times into M9 Glucose minimal media, to get a working solution of 10$\mu$g/ml A22.

### 2.3.4 Bending Protocol

For a maximal output and a successful implementation of the bending protocol, the sample preparation was always conducted for two sample slides. Because of the influence of A22 to cell growth and the length of the cells, a single slide was not used for more then 3h. After sample placement, an appropriate cell with a length between 9-20$\mu$m was selected. For multiple reasons, such as to ensure a negligible stretching force, to simplify later image analysis or to ensure the before calibrated laser stiffness was still valid, cells had to match the following criteria: Only rod cells were considered which had a clear defined stuck end and free end. The stuck end was completely attached to the surface and did not show any movement after trapping the free end. The length of the stuck end was not smaller than 3$\mu$m. One main selection criteria was concerning the distance of the free hanging tip of the cell to the surface. The laser stiffness decreases over the distance to the surface [14], and therefore the tip of the cell was maximal 2.5$\mu$ away from the surface. To avoid the tip of the cell attaching to the surface after injection of the polysterene beads or A22, a minimal distance of 200nm was chosen. If an appropriate cell was found, a mixture of poly-Lysine coated polysterene beads and M9 Glucose Minimal Media (1: 6000) was injected into the microfluidic channel. After the surplus liquid was removed, a single polysterene bead was trapped and attached on the side of the free hanging end of the cell. After multiple calibration steps, the attached cell was trapped with optical tweezers and bend in an rectangular angle via moving the sample stage. The displacement of the attached bead to the focus point of the optical trap was measured and a force-displacement curve was generated (Figure 8 / Force Displacement). This step was repeated twice to get 3 several bending measurements of a single cell. During the next step, 40 $\mu$l of a A22 0.2% BSA M9 Glucose solution was injected into the channel. After 2-3min the MreB was depolymerized and another 3 bending measurements were taken. After all, A22 was removed with 40l M9 Glucose minimal medium and another appropriate cell was seek. This procedure allowed us to measure up to 5 cells per slide.

## 2.4 Width Measurements of MreB Mutants

To ensure our later described correlation between bacterial cell width and bending stiffness was valid, multiple width measurements with fluorescence microscopy techniques were conducted. Various reasons, such as switching of growth media condition, using PEI as a surface binder and the Cephalexin treatment to induce filamentous growth supported the decision to re-measure existing cell diameters. For all experiments, *E. coli* cells were prepared in the same way as for the bending experiments to ensure similar environmental conditions. One crucial difference during the final incubation step was applied. To gain similar cell length, all cells were grown 120min at 37 ° after the cell surface attachment occurred. Afterward, cells were labeled with with the fluorescence dye FM4-64 (Invitrogen). Therefore, FM4-64 dye in a concentration of 500$\mu$g/ml was diluted 500 times in 0.2% BSA M9 Glucose solution. Finally the microfludic channel was floated with 100$\mu$l of the prepared FM4-64 media solution and used for later fluorescence imaging. During fluorescence imaging, only bacterial cells were considered which matched the same criteria as set for the bending protocol. Cells need to have an appropriate free end length and are supposed to be smaller then 20$\mu$m in total length. We also considered cells that were more then 2.5$\mu$m away from the surface, as long as they were able to measure. For the fluorescence measurements, a stack between 100 to 150 planes in z-direction was recorded. This allowed us to get a theoretical 3 dimensional image of the cell, based on the membrane labeling with FM4-64 (Figure 7). All cells were finally analyzed by costum-written Matlab programs and image processing tools (Width Calibration and Calculation).

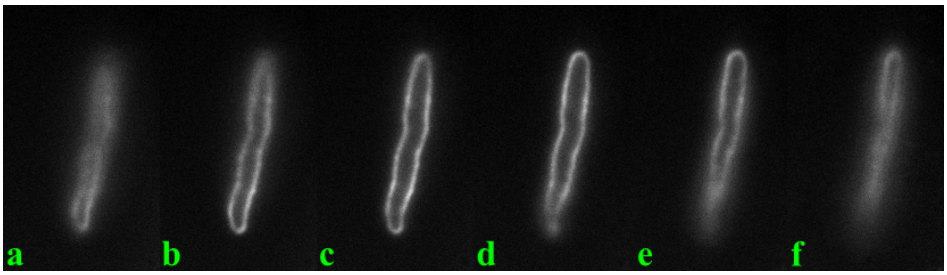


Figure 7: (a-f) Fluorescence stack of mreB mutation A53T. Distances between each image are approximately 200nm. Cells were labeled with the fluorescence dye FM4-64 and indicate a helical shape.

## 2.5 Working Principles and Computational Analysis

### 2.5.1 Force Displacement and Calibration

The goal of our bending measurements was to gain the flexural rigidities of selected strains and to compare and connect differences in multiple mreB mutations. To do so, we used optical tweezers to measure the force it needs to bend a single cell. The force measurement could be conducted with an optical set up in the way, that we use two different optical tweezers. The first laser (1064nm) was used to induce the cell bending and a weaker second detection laser (582nm) was implemented to observe a possible bead displacement from the focus point of the trapping laser. To measure this before mentioned displacement, it was necessary to overlay and calibrate both optical tweezers. The calibration [8,9,15,37] was conducted with costum-written Labview programs and the goal was to determine the laser stiffness of the

$$d_{stage} = d_{bead} + d_{cell} \tag{1}$$

1064nm laser. All force measurements used these calibrated values and allowed us to determine the exact force for a bead displacement in the optical trap. Also, both lasers were overlayed by using custom-written Labview programs. The working principle of the laser detection can be easily summarized in two steps. First, a cell with an attached bead was trapped and moved perpendicular to the cell axis. The total stage movement was the sum of the bead and cell tip displacement (1). A force displacement curve in x and y direction was recorded and summarized in a singe plot (Figure

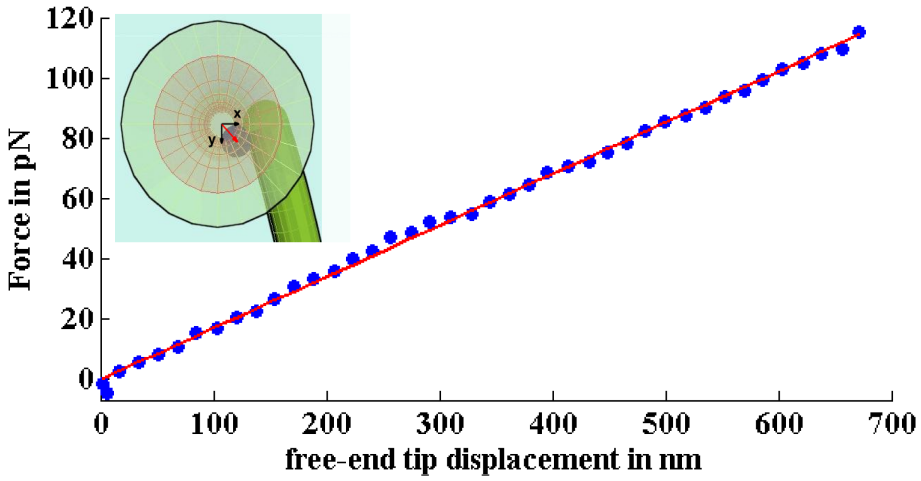


Figure 8: Linear force- displacement curve of a bend cell. The force curve is for all strains linear and only the force and displacement values differ. (top left) Illustration of a bead displacement during bending. Two force curves in x and y direction were generated and summarized in one (red arrow)

8). Therefore, this technique allows us to determine and record an accurate cell tip displacement and force measurement over time. The final output was a force- cell tip displacement curve, induced by the bending.

### 2.5.2 Computational Image Analysis

The image analysis marks the last part of each bending experiment. It combines the determined force-displacement values with the recorded images of the bending. Therefore two images of each bending were compared to each other. The first image marks the beginning of each bending of a cell in a relaxed state with the trapped attached bead. The second showed the cell

$$y(z) = \begin{cases} \frac{F}{EI}\left[\frac{L(L-z)^2}{2} - \frac{(L-z)^3}{6}\right], z < L \\ 0, z > L \end{cases} \quad (2)$$

in the bend state. Bent cells were not always perfectly rod shaped and would be hard to compare with each other. Therefore, costum- written Matlab programs, using the Canny edge detector for grey-scale DIC images, were used to determine a center line of a each cell before and after the bending (suppl.[3]). Both center-lines were finally overlayed and compared with each other. The resulting data points were fitted, using a theoretical fit function (2) for a bend rod with a stuck end (Figure 9). In this equation (2), F represents the applied bending force, EI the flexural rigidity, L the free end length of the cell and z marks the arc length of the cell. In the end, the force displacement values and analyzed image data could be combined and final values for the flexural rigidity and free end length were determined.

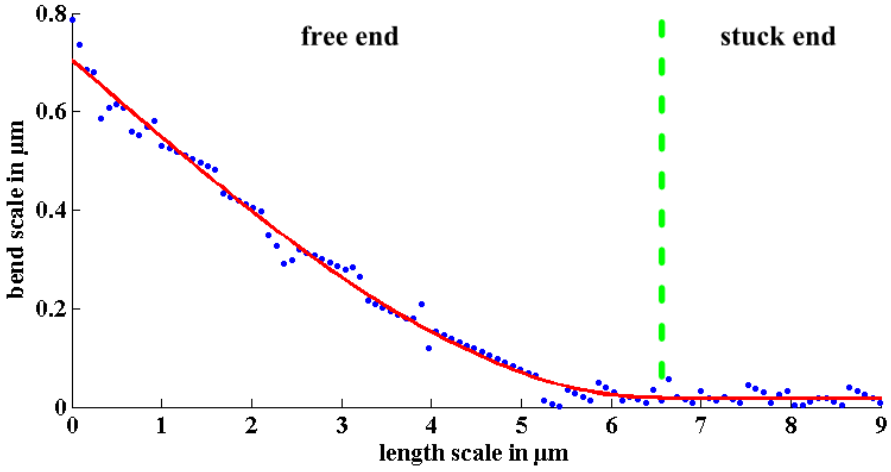


Figure 9: Here, the final bend values of a single bend is shown. x and y scales are in $\mu$m. All data points were plotted after combination of the relaxed and bent state of a single cell (blue). A theoretical fit (2) of all data points were applied and the free end length could be determined (left).

### 2.5.3 Width Calibration and Calculation

Bacterial cells from different strains differ in size. Previous width measurements of all investigated strains showed a difference in size as a direct result of various mutations in mreB. The width resp. the radius of each strain was a main concern and due to may induced changes in size because of changes in media condition, surface coating with PEI or the use of Cephalexin to induce filamentous growth, an additional more accurate width measurement was conducted. The data of the previously described fluorescence experiment was then analyzed computationally. To ensure the recorded images of the cells, tagged with the fluorescence dye FM4-64, show an accurate maximum width, we calibrated our image analysis with simulated, well known 2D images of cylinders with various diameters. A simulated stack of 75 images of 9 cylinder of differing sizes were used to calibrate later width measurements. As a result of the FM4-64 staining, tagged cylinders were bigger than they appeared under confocal fluorescence microscopy. A simple explanation for this effect is described in Figure 10. Because of the cylindrical shape, the used fluorescence dye is located all around the cell and influences the maximum peak in this way, that it appears more inside the cylinder. The observed diameter was therefore smaller in comparison to the real diameter. In the middle of each cylinder and where the resulting peaks show the biggest distance, plot profiles were taken over the whole diameter of a cell. Because of an optical resolution of minimal 80nm per pixel and to gain a more precise width measurement, the resulting plot profiles where fitted with a double Gaussian to overcome the resolution barrier (3). The parameters $a_1$ and $a_2$ mark the amplitude of each peak, $b_1$ , $b_2$ the position on the x-axis and $c_1$ and $c_2$ the width of each

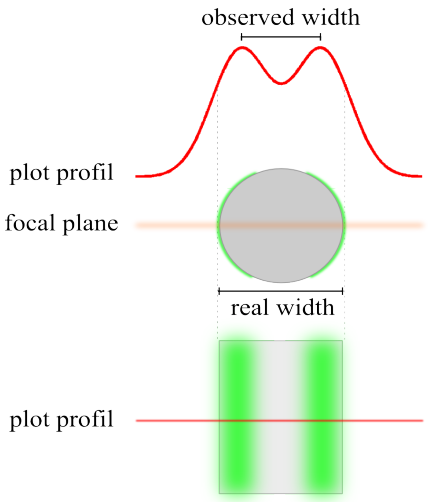


Figure 10: Cylindrical shaped object from top and side view. Analyzed images were located in the middle of the cylinder resp. cell. The resulting profile plot were fitted using a double Gaussian and show a discrepancy in width. Fluorescence labeled rod shaped objects appear smaller.

$$y(x) = a_1 e^{-\left(\frac{x-b_1}{c_1}\right)^2} + a_2 e^{-\left(\frac{x-b_2}{c_1}\right)^2} + d_{off} \tag{3}$$

peak. $d_o$ff describes a background noise induced offset of the double Gaussian fit. The difference of the resulting positions of each peak maximum was

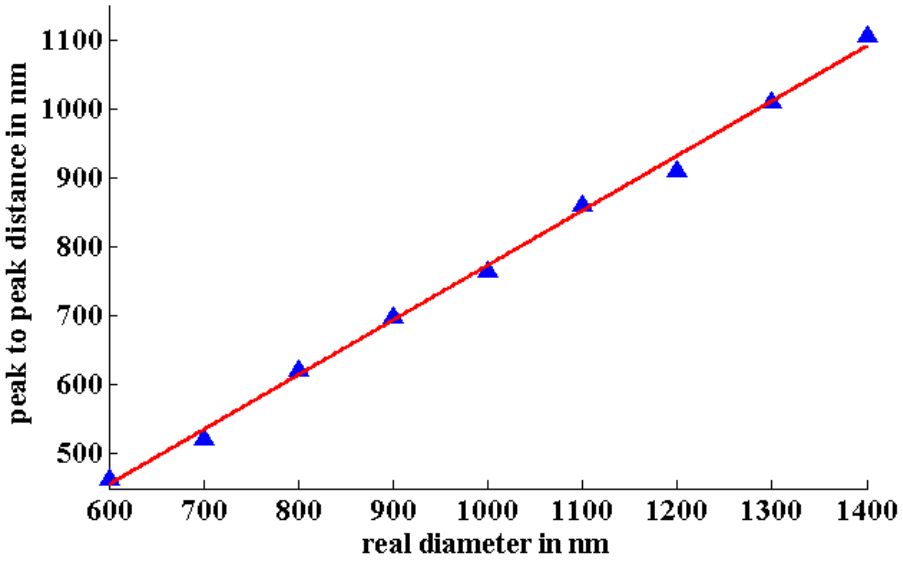


Figure 11: Calibration plot for all bacterial width measurements using confocal fluorescence microscopy. Here shown is the real diameter of a cylindrical shaped object vs. its observed diameter after image analysis.

used to obtain the width of each cylinder resp. cell. The known diameters of each cylinder was then plotted against the observed diameter and linear fitted (Figure 11). Finally, the fit was used to correct all width measurements of investigated bacterial strains. Afterward, the same protocol was applied for all measurements on bacteria. In summary, a single image of the middle of the cell in z-direction was chosen and a plot profile was taken. The profile data was fitted with a double Gaussian and differences in peak distances were measured. The resulting observed widths were finally converted into real diameters using the previously calibrated width of simulated cylinders.

# 3 Results and Discussion

## 3.1 Change in Cell Stiffness with and without MreB bundles

### 3.1.1 Bending Results with and without A22 Treatment

The application of the bending assay allowed us to measure the flexural rigidities and stiffness of the B-strain and the corresponding mutations in mreB. We have demonstrated that the modified sample preparation including the bending protocol can be used to determine mechanical properties of single cells under specific conditions. Single measurements on different cells show a decrease of the bending stiffness after A22 treatment and a recovery to normal stiffness values after removing the drug A22. Therefore, the drug A22 inhibits MreB polymerization by blocking the ATP binding pocket. The polymerization of MreB filament is an ongoing process and the descibed effect of A22 leads indirectly to a depolymerization of MreB filaments [2]. The depolymerization takes several minutes and conducting measurements took place after the depolymerization was complete. Bending measurements by Siuyan Wang [3] indicate a depolimerization time of approximately 2-4 minutes. We applied his former measurements and waited 2-3 minutes before measuring the influence of A22 on bending stiffness. The results for a single cell are shown in figure 12. Three different histograms show the flexural rigidities of a single wild type cell before A22 treatment, with A22 and the recovery after A22 was removed. After A22 was removed bacterial cells re-

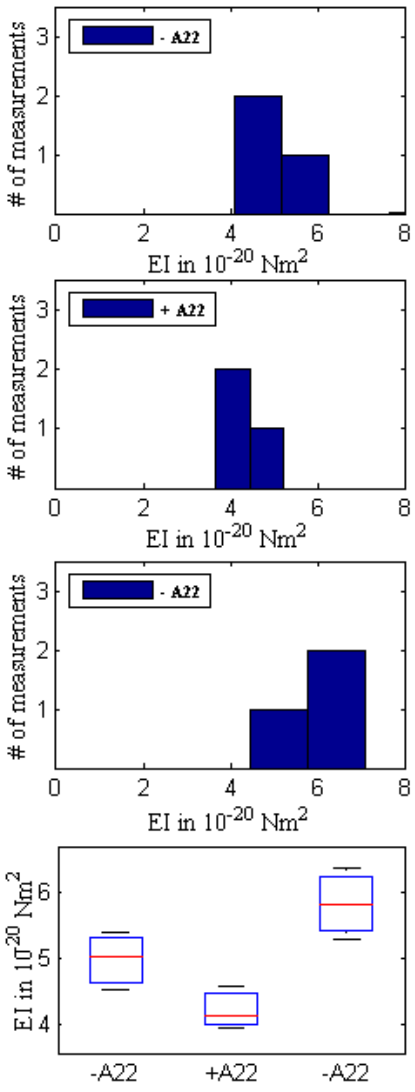


Figure 12: Histograms for a single wild type cell indicate a change in flexural rigidity with and without MreB bundles. After the remove of A22, start values of the flexural rigidity were reached again. A summary of all median values is illustrated in the graph below.

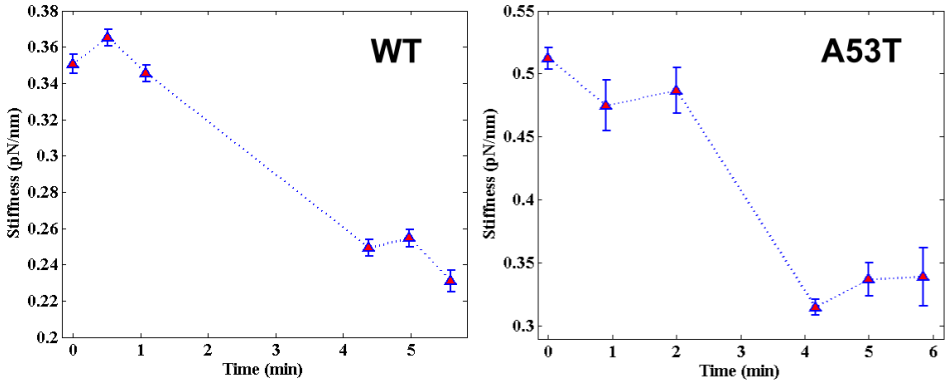


Figure 13: Single experiments before and during A22 treatment of a single wild type cell (left) and a cell with a mutation in mreB-A53T (right). For each stage, three independent measurements were taken and show a decrease in the relative stiffness of each cell. The time in between each stage was chosen as approximately 3 minutes.

cover and show similar values for the flexural rigidity. The median values show clear differences during this procedure (Figure 12 bottom). The smaller EI values are directly caused by a smaller bending force without MreB. Besides changes in the flexural rigidity, also differences in the relative stiffness of single bacterial cells could be observed. Figure 13 shows differences in relative stiffness over time in case of the wild type B-strain and mreB-A53T mutant. The gap in between both triplets describes the minimal time until MreB depolymerizes completely. The relative stiffness depends on the slope of a single force-displacement curve (Figure 8) and was different because of differences in the free end length of each cell. As with the relative stiffness, the flexural rigidity is cell length independent and just the free end length in relation to the radius of a cell contributes to mechanical bending properties.

| **Strain** | **Flexural rigidity** | |
|---|---|---|
| | **$-$A22 [$10^{-20}$Nm$^2$]** | **$+$A22 [$10^{-20}$Nm$^2$]** |
| **wild type** | $\mathbf{4.98 + -1.29}$ | $\mathbf{3.97 + -1.52}$ |
| **mreB-A53T** | $\mathbf{25.18 + -10.36}$ | $\mathbf{19.99 + -8.40}$ |
| **mreB-A53T L322Q** | $\mathbf{5.45 + -0.95}$ | $\mathbf{4.66 + -0.77}$ |
| **mreB-A53T G207C** | $\mathbf{4.33 + -1.45}$ | $\mathbf{3.55 + -0.93}$ |
| **mreB-A53T L209R** | $\mathbf{2.91 + -1.20}$ | $\mathbf{2.66 + -1.25}$ |
| **mreB-L322Q** | $\mathbf{2.88 + -0.74}$ | $\mathbf{2.32 + -0.74}$ |
| **mreB-G207C** | $\mathbf{8.74 + -0.45}$ | $\mathbf{6.49 + -0.01}$ |

Table 2: Summary of measured B-strains and the EI values before and during A22 treatment. A significant decrease between 8-20% was observed.

Multiple histograms of all observed values for the flexural rigidity are shown

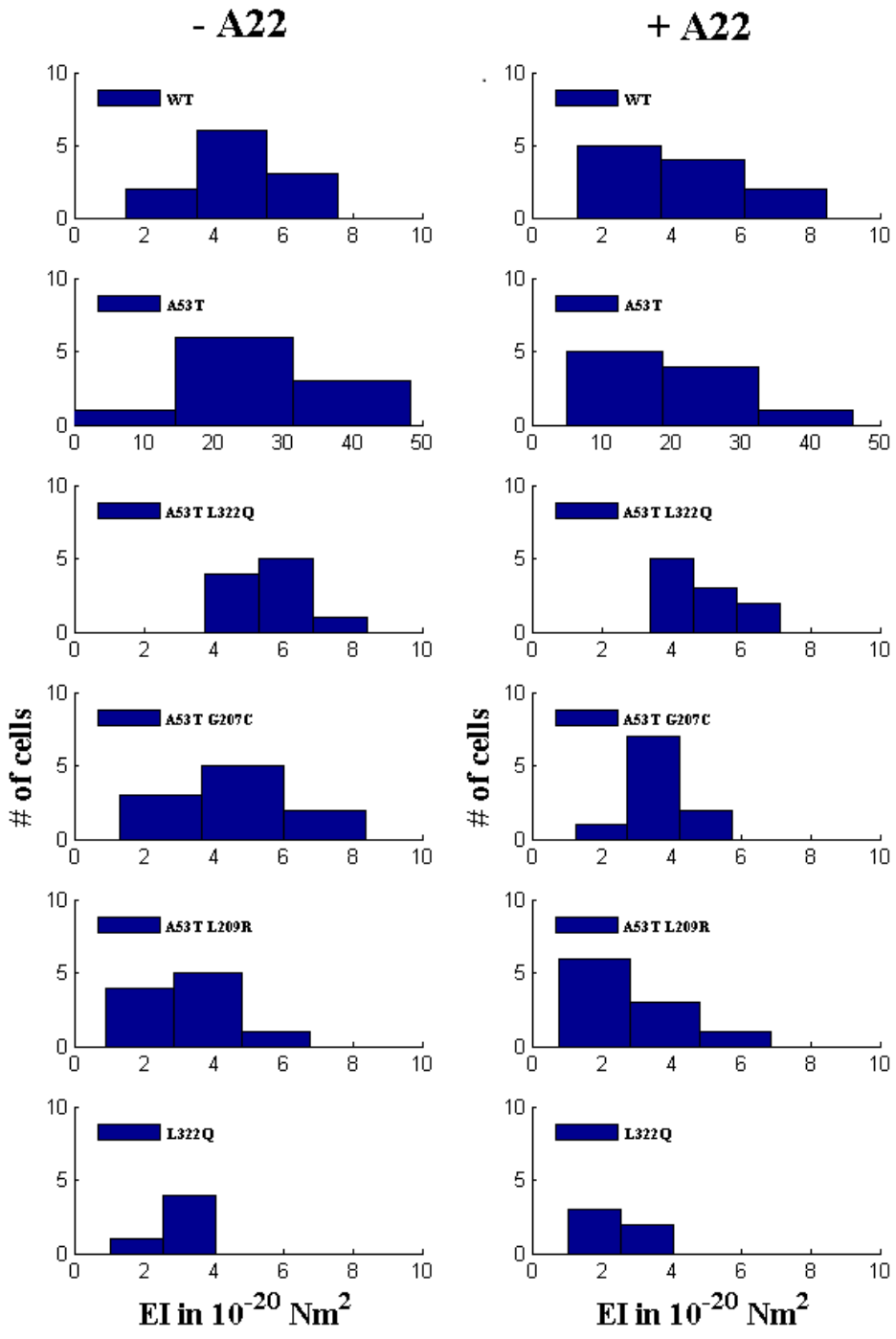


Figure 14: The measured flexural rigidities of the wild type B-strain and all mreB mutants are shown in each histogram. All EI values before A22 treatment (left) and during A22 treatment (right) are shown in both columns. 5-12 cells were measured per strain and decreases in bending stiffness are clearly visible. The bin width was calculated by Scotts normal reference rule [32].

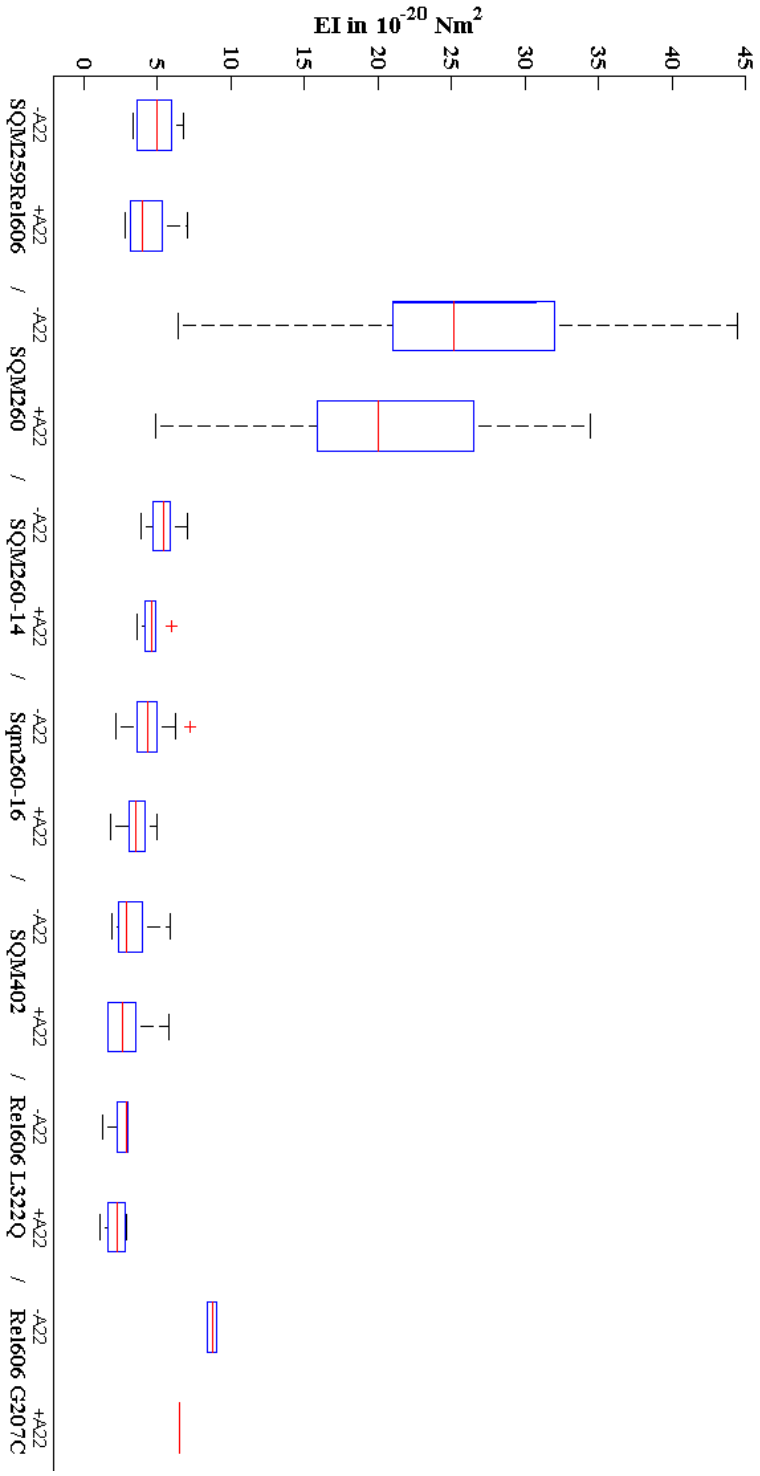


Figure 15: Summary of all measured strains. The median values (red) show clear defined differences between each *E.coli* strain. Each doublet stands for a used strain with and without A22 treatment.

in Figure 14. For the wild type B-strain (n=11), we observed a decrease of the flexural rigidity during A22 treatment from $4.98 + -1.29\text{Nm}^2$ before A22 treatment to $3.97 + -1.52\text{Nm}^2$ after A22 was injected in the device. The influence of MreB on bending stiffness in the B-strain is about 20%. To compare the mechanical properties of the mreB bundles, measurements for all mreB mutants were conducted. Thereby, the single point mutant in mreB-A53T show an huge increase in bending stiffness. We observed an almost 5 times higher median value for the flexural rigidity. In numbers, A53T (n= 10) bending stiffness decreased from $25.1783 + -10.36\text{Nm}^2$ to $19.99 + -8.4\text{Nm}^2$ after depolymerization of mreB bundles. The maybe destabilized MreB polymers increase not just the diameter of the cells, also the mechanical properties are significantly different for this mutation. In addition to the single A53T mutant, double point mutations with a second suppressor mutation in mreB were analyzed and show similar values as the wild type for bending stiffness. In detail, A53T L322Q (n=10) show a decrease from $5.45 + -0.95\text{Nm}^2$ to $4.66 + -0.77\text{Nm}^2$, A53T G207C (n=10) a decrease from $4.33 + -1.45\text{Nm}^2$ to $3.55 + -0.93\text{Nm}^2$ during A22 treatment and A53T L209R (n=10) a decrease from $2.91 + -1.20\text{Nm}^2$ to $2.66 + -1.25\text{Nm}^2$. To control the influence of the suppressor mutations L322Q and G207C which lead to a normalization of bending stiffness, we applied the bending protocol for these strains as well. mreB-L322Q (n=5) show a reduce in stiffness of approximately 20%, from $2.884 + -0.74\text{Nm}^2$ to $2.32 + -0.74\text{Nm}^2$ and mreB-G207C (n=2) from $8.74 + -0.45\text{Nm}^2$ to $6.49 + -0.01\text{Nm}^2$. The observed flexural rigidities for all strains in detail are summarized again in Table 2 and illustrated in Figure 15. Each strain shows clear differences with and without A22 treatments. In detail, differences concerning bending stiffness of each strain individually is summarized in figure 17 (detail Appendix Fig.1). A linear increase proportional to the increasing flexural rigidities could be observed.

### 3.1.2 Interpretation and Conclusion

A22 and the loss of mreB through inhibiting polymerization changes the overall stiffness of bacterial cells. In comparison to former measurements by Siuyen Wang [3] who showed that MreB contributes almost 30% to the overall stiffness of *E.coli* WA220 cells, we measured differences between 8-20% with and without MreB. Differences can be explained by variations in bacterial background, sensitivity to A22 [7] or individual mutations in mreB. The used protocol showed also differences in media condition, which most likely led to an increased diameter of the cell [26]. The diameter of a single cell is one major component of the flexural rigidity (7) and needs to evaluate individually in combination with the bending stiffness of each strain. In general, the contribution of MreB to cell stiffness fits with our current model. Less then 10 MreB filaments per micrometer with strain depended variation in polymer length between a couple of hundred nanometers to one micrometer support our data. One important, but widely unknown phenomena is based on the question: How does MreB contribute its part to cell stiffness. One possibility would rely on the polymer stiffness itself. MreB is located on the inside of the inner membrane and could increase stiffness as a second shape-determining structure. A different and more likely possibility to explain this effect is based on a undefind connection of MreB to the peptidoglycan through an inner membrane protein such as MreC or RodZ [30-31] (Figure1). MreB could bind to the PG in an unknown way and therefore support and increase cell stiffness indirectly as a second part of the shape determine peptidoglycan. Both scenarios are possible, but a definite explanation cannot be given because many aspects of MreB are still widely unknown. Another interesting part of our measurements are based on individual applications of the bending protocol to each mreB mutation. Some aspects of the applied protocol such as Cephalexin treatment or media change led to changes in cell shape and size of some mreB- mutants. In case of the single point mutant A53T, different cell defects were observed over time, most likely induced by the filamentous growth through Cephalexin (Figure 16b). Defects like this were also observed by our col-

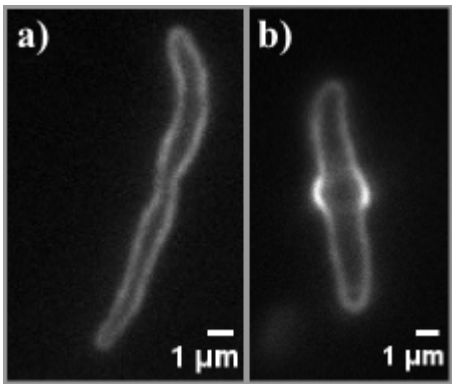


Figure 16: Possible defects in shape of mreB-A53T G207C (a) and mreB-A53T (b). These defects occur sporadic and under different condition. While the size differences in G207C are most likely induced by a change in media condition, the defect in A53T relies on the induced filamentous growth due to Cephalexin treatment after 1-3 hours.

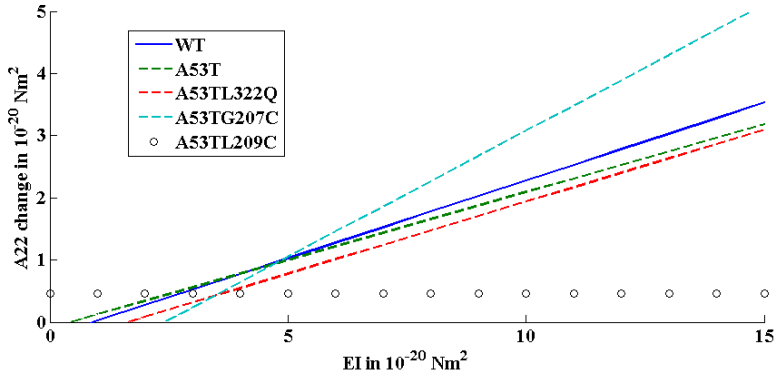


Figure 17: Changes in flexural rigidity after A22 treatment. The fitted plots illustrate the change in bending stiffness for each strain. Negative values were excluded. A linear increase could be observed.

laborator K.C.Huang [22]. This observation supports our theory that the A53T mutation in mreB destabilizes the MreB polymer. A second observed phenomena occurred in the suppressor mutant G207C. In both, single and double mutant with A53T, a change in cell width could be observed. In comparison to other strains, in some cases differences in cell width of more than 50% within one single cell could be observed (Figure16a). This effect was most likely induced due to a media change from LB to M9 Glucose minimal media and demonstrates that single point mutations in mreB can cause huge differences in cell width depending on the media condition. For our measurements, just cells with a smoother shape were chosen, to minimize variations in flexural rigidity. In addition to possible explanations about how MreB contributes to stiffness, we decided to investigate in stiffness differences between each measured strain. The wild type strain and all mreB mutants differ in size and bending stiffness. Therefore we analyzed the correlation of both to get an idea about the function and resulting effect of different mutations in mreB on the mechanical properties of a cell.

### 3.2 Correlation between Bending Stiffness and Cell Radius

The mechanical properties of bacterial cells depend strongly on their type and species. Here, we focused on differences within the *E.coli* B-strain in comparison to various mreB mutants. Therefore, basic formulas to describe the bacterial stiffness had to be selected. The stiffness k of a single rod can be described by:

$$k = 3\frac{EI}{L^3} \tag{4}$$

Thereby, EI describes the flexural rigidity and L the length of the bend rod. Here, L marks the free end length of a single bacterial cell. The flexural rigidity EI can be described as a product of the Young modulus E (5) and second moment of inertia I (6).

$$E = \frac{FL_0}{A_0 \Delta L} \tag{5}$$

F represents hereby the applied bending force, $L_0$ the free end length of the bend rod, $A_0$ the cross-section and $\Delta L$ the change in length through bending or the elastic change in length. For a thin hollow cylinder, the second moment

$$I = \frac{1}{4}\pi[R^4 - (R-b)^4] \approx \pi R^3 b \tag{6}$$

of inertia describes a geometrical property of an area which consists of two parameters, the radius of the rod R and the thickness of the cylinder b. In the provided model, a rod shaped cell has a constant volume and can be seen as a thin hollow cylinder. The shape determined thin shell would represent the peptidoglycan structure and MreB would act as a supporting parameter as part of the cell wall the cell wall. As a combination of (5) and (6), the flexural rigidity can be expressed as:

$$EI = Eb\pi R^3 \tag{7}$$

To prove, if differences in bending stiffness are caused by structural changes within the cell wall or are results of a change in cell width, induced by mutations in mreB, measured flexural rigidities can be compared to cell widths of individual strains. As a direct result of (7) the correlation between bending stiffness and cell radius can be described as

$$EI \propto R^3 \tag{8}$$

To do so, cell widths were calibrated with simulated cylinders of various size and measured with confocal fluorescence microscopy to overcome possible changes in cell width, induced by changes in media conditions, PEI surface coating or Cephalexin treatment.

### 3.2.1 Cell Width Measurements and Calibration

As a core factor for a good understanding what mutations in mreB are doing, cell widths were measured under the conditions of the bending protocol. Problems with differences between observed and real diameter were solved by applying before calibrated widths of simulated cylinders (Figure 11). The resulting cell diameter of each strain can be seen in Table 3. As mentioned before, mutations in mreB causes bacteria to produce cells with different width. A reason for that could be found in preliminary data by Nick Ouzounov in the group of Prof. Zemer Gitai [58]. Recent data show a correlation between MreB polymer lengths and cell width. Longer MreB polymers seem to result in thinner cells, and vise verca. Therefore, differences in cell width induced by specific single or double point mutations in MreB could lead to differences in polymer lengths of MreB. Additional factors like polymer orientation, twist or bending are not included. To control if the mechanical properties and functions of MreB are different as well, we applied all measured flexural rigidities and compared them to the width of individual strains (MreB vs. Cell Wall Structure).

| **Strain** | **Cell Width [nm]** |
|---|---|
| **wild type** | $\mathbf{930.2 + -56.9}$ |
| **mreB-A53T** | $\mathbf{1425.9 + -133.4}$ |
| **mreB-A53T L322Q** | $\mathbf{985.3 + -45.9}$ |
| **mreB-A53T G207C** | $\mathbf{924.3 + -77.8}$ |
| **mreB-A53T L209R** | $\mathbf{867.9 + -55.9}$ |
| **mreB-L322Q** | $\mathbf{725.6 + -79.2}$ |

Table 3: Calculated cell width after calibration adjustments.

### 3.2.2 MreB vs. Cell Wall Structure

The collected data for the flexural rigidities and cell width were now used to prove if specific mutations causes structural changes in the composition and construction of the peptidoglycan cell wall. As widely known, MreB colocalizes with the cell wall syntheses [36]. From equation (7), three possible parameter could be responsible for changes in the flexural rigidity of bacterial strains. Changes in the young modulus E or the cell wall (PG) thickness b would indicate a functional influence of MreB on cell wall syntheses. Therefore, MreB would be responsible for insertion of cell wall material and differences in width and flexural rigidity could rely on changes

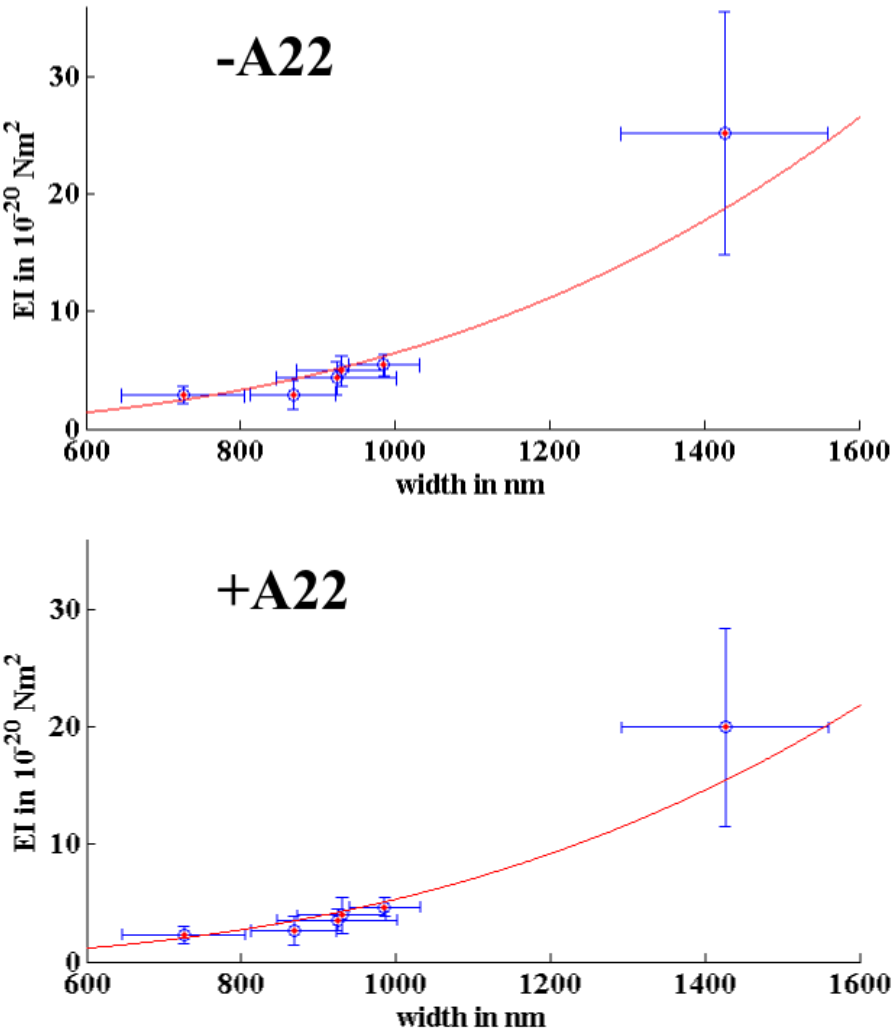


Figure 18: Here, the measured cell width of each strain is plotted against the data of the flexural rigidity. Errorbars in x and y indicated the standard deviation of width and EI. The data was plotted with equation (7) (red).

in the peptidoglycan structure itself, such as glycan length or PG thickness in terms of multilayer. Surprisingly, the opposite was the case. Changes in flexural rigidity of each strain seem just to be based on the different cell radia. Figure 18 shows the correlation between cell width and bending stiffness. After fitting our current model $Eb\pi R^3$ (red) to the collected data, a clear radius dependency was observed. A result of this indicates a functional property of MreB. It seems like, that due to the colocalization of MreB to cell wall synthesis, MreB is just responsible for the localization of cell wall material and synthesis and not for the insertion itself. Preliminary data form our collaborators at Stanford University, Prof. K.C. Huang and Russel Monde, support our data. Due to HPLC measurements on peptidoglycan of the same bacterial strains, no large changes in composition and amount of peptidoglaycan could be observed [59]. Therefore, the cell wall thickness seems to be the same in the mreB mutants and the variations of bending stiffness are clearly depending on the individual radius of each strain. As a control, we calculated the resulting $Eb$ values for the radius dependency, using model (7). Under the assumption, cell wall thickness is the same in each mutant, we assume the thickness of a single peptidoglycan layer with approximately 4 nm [28]. The Young modulus perpendicular to the cell axis can be now estimated with $E_{noA22} = 41.16$ MPa without A22 treatment and $E_{A22} = 33.92$ MPa during A22 treatment. Almost 25% of the Young modulus would be contributed by MreB. Estimated Young moduli by Yi Deng and Prof. Joshua Shaevitz at Princeton University using atomic force microscopy techniques show similar values for *E.coli* between 20-45 MPa, depending on Young modulus orientation [11,36]. Differences in bending stiffness can now be explained with proportional changes in cell diameter, but reasons for changes in cell diameter in cells with mreB mutations remain still unclear. A possible reason could be previously described changes in polymer length, orientation, twist or bending of MreB [24]. A bending of MreB filaments would be caused by changes in the angle between two connected monomers as well as twisting. To verify our theories, more experiments have to be conducted. The investigated strains show an huge gap in cell width, and mreB mutants should be uncovered to close the gap and support our current model.

# 4 Conclusion and Future Perspectives

Many questions about MreB and its function remain unknown, but here, we could provide data which indicates a functional behavior of the actin equivalent MreB. It was shown and replicated the result that the drug A22 leads to a decrease in flexural rigidity and cell stiffness of 8-20%. Therefore, MreB contributes a significant amount to cell stiffness and we could reproduce former experiments [3]. A modification of the existing bending protocol improves the measured cell per day ratio and also physical properties of the bending assay itself. Additional measurements on the wild type B-strain and specific mutations in mreB could be measured and differences in bending stiffness within each mutation could be shown. The mreB-A53T mutant show an incredible high flexural rigidity and indicated a cell width dependency of the bending stiffness. Later measurements and analysis support our former data and show, that the model $EI \propto R^3$ can be applied. The Young modulus with and without MreB bundles could be estimated and a new hypothesis concerning the function of MreB was provided. The shown data indicates that MreB is just responsible for the localization of cell wall material and not for the construction of the cell wall itself. Upcoming experiments in terms of bending or cell stiffness have to be conducted to support our current model of MreB a guide for peptidoglycan synthesis.

# 5 Acknowledgement

I would like to thank Prof. Joshua Shaevitz and his group at Princeton University for their great support and the opportunity to work on this exciting project for 12 months in his laboratory. Thanks to Benjamin Bratton and Jeffrey Nguyen for their help, support and patients over the whole time in Princeton. Also thanks to Prof. Zemer Gitai and his group for the critical discussions and great input. Also grateful acknowledged are our Collaborators at Stanford University Prof. KC Huang and Russel Monde, Siyuan Wang for his previous work and help, as well as Nikolay Ouzounov for helpful discussions of biological questions and Sven van Teeffelen. Finally I would like to thank the people and organizations who made this project possible: my home Advisor Prof. Thomas Pfohl and former Advisor Prof. Urs Jenal from the University of Basel, as well as the Swiss Nanoscience Institute and the University of Basel for the financial support. Thanks to PhD candidate Angelina Sylvain from Princeton University for editing this thesis.

## References


[1] A novel membrane-bound toxin for cell division, CptA (YgfX), inhibits polymerization of cytoskeleton proteins, FtsZ and MreB, in Escherichia coli, Hisako Masuda, Qian Tan, Naoki Awano, Yoshihiro Yamaguchi and Masayori Inouye, *FEMS Microbiol Lett*(2012) 328, 174181

[2] A22 Disrupts the Bacterial Actin Cytoskeleton by Directly Binding and Inducing a Low-Affinity State in MreB, G. J. Bean, S. T. Flickinger, W. M. Westler, M. E. McCully, D. Sept, D. B. Weibel and K. J. Amann *Biochemistry*(2009) DOI:10.1021/bi900014d

[3] Actin-like cytoskeleton filaments contribute to cell mechanics in bacteria, Siyuan Wang, Hugo Arellano-Santoyo, Peter A. Combs, and Joshua W. Shaevitz, PNAS (2010), vol.107, no.20, 91829185

[4] Bacillus subtilis MreB paralogues have different filament architectures and lead to shape remodelling of a heterologous cell system, Herv Jol Defeu Soufo and Peter L. Graumann, *Molecular Microbiology* (2010) 78(5), 11451158

[5] Bacterial actin MreB assembles in complex with cell shape protein RodZ, Fusinita van den Ent, Christopher M Johnson, Logan Persons, Piet de Boer and Jan Lwe, *The EMBO Journal* (2010) 29, 10811090

[6] Cell shape and cell-wall organization in Gram-negative bacteria, Kerwyn Casey Huang, Ranjan Mukhopadhyay, Bingni Wen, Zemer Gitai, and Ned S. Wingreena, PNAS (2008), vol.105, no.49, 1928219287

[7] Characterization of a novel antibacterial compound A22, Simon Hockenhull, Wei Shi and Rasmus Bugge Jensen, Department of Life Sciences and Chemistry, Roskilde University, 2006

[8] Quantifying Noise in Optical Tweezers by Allan Variance, Fabian Czerwinski, Andrew C. Richardson, and Lene B. Oddershede, OPTICS EXPRESS (2009), vol.17, no.15, 13255

[9] Optimizing active and passive calibration of optical tweezers, MAndersson, F Czerwinski and L B Oddershede, *J. Opt.* (2011) 13, 044020 (6pp)

[10] Determination of bacterial rod shape by cytoskeletal membrane protein, Daisuke Shiomi, Masako Sakai and Hironori Niki, *The EMBO Journal* (2008) 27, 30813091

[11] Measurement of CellWall Stress Stiffening and Turgor Pressure in Live Bacterial Cells, Yi Deng, Mingzhai Sun, and Joshua W. Shaevitz, PRL (2011) 107, 158101

[12] Direct Measurements of Heating by Electromagnetically Trapped Gold Nanoparticles on Supported Lipid Bilayers, Poul M. Bendix, S. Nader S. Reihani and Lene B. Oddershede, ACS Nano (2010) vol.4, no.4 22562262

[13] Direct Membrane Binding by Bacterial Actin MreB Jeanne Salje, Fusinita van den Ent, Piet de Boer, and Jan Lwe, *Molecular Cell* (2011) 43, 478487

[14] An Integrated Laser Trap/Flow Control Video Microscope for Study of Single Biomolecules; Gijs J.L.Wuite, R.JohnDavensport, Aaron Rappaport and Carlos Bustamente Biophysical Journal Vol.79 , August 2000 1155-1167

[15] Active-passive calibration of optical tweezers in viscoelastic media, Mario Fischer, Andrew C. Richardson, S. Nader S. Reihani, Lene B. Oddershede and Kirstine Berg-Srensen, REVIEW OF SCIENTIFIC INSTRUMENTS (2010) 81, 015103

[16] From individual cell motility to collective behaviors: insights from a prokaryote, Myxococcus xanthus, Yong Zhang, Adrien Ducret, Joshua Shaevitz and Tam Mignot, FEMS Microbiol Rev (2012) 36, 149164

[17] From the regulation of peptidoglycan synthesis to bacterial growth and morphology, Athanasios Typas, Manuel Banzhaf, Carol A. Gross and Waldemar Vollmer, *Nature Review Microbiology* (2012), vol.10

[18] Helical insertion of peptidoglycan produces chiral ordering of the bacterial cell wall, Siyuan Wang, Leon Furchtgott, Kerwyn Casey Huang, and Joshua W. Shaevitz, 10.1073/pnas.1117132109

[19] Image analysis in fluorescence microscopy: Bacterial dynamics as a case study, Sven van Teeffelen, Joshua W. Shaevitz and Zemer Gitai, Bioessays (2012) 34, 427436

[20] Lights, action: optical tweezers, JUSTIN E. MOLLOY and MILES J. PADGETT, *Contemporary Physics* 2002, vol.43, no.4, 241-258

[21] Measuring the stiffness of bacterial cells from growth rates in hydrogels of tunable elasticity, Hannah H. Tuson, George K. Auer, Lars D. Renner, Mariko Hasebe, Carolina Tropini, Max Salick, Wendy C. Crone, Ajay Gopinathan, Kerwyn Casey Huang and Douglas B. Weibel, *Molecular Microbiology* (2012) 84(5), 874891

[22] Mechanisms for maintaining cell shape in rod-shaped Gram-negative bacteria, Leon Furchtgott, Ned S. Wingreen and Kerwyn Casey Huang, *Molecular Microbiology* (2011), 10.1111/j.1365-2958.2011.07616.x

[23] Morphology, Growth, and Size Limit of Bacterial Cells, Hongyuan Jiang and Sean X. Sun, PRL 105, 028101 (2010)

[24] MreB: pilot or passenger of cell wall synthesis?, Courtney L. White and James W. Gober *Trends in Microbiology*(2012), Vol. 20, No. 2

[25] MreB, the cell shape-determining bacterial actin homologue, coordinates cell wall morphogenesis in Caulobacter crescentus, Rainer M. Figge, Arun V. Divakaruni and James W. Gober, Molecular Microbiology (2004) 51 (5), 13211332

[26] Phenotypic Landscape of a Bacterial Cell, Robert J. Nichols, Saunak Sen, Yoe Jin Choo, Pedro Beltrao, Matylda Zietek, Rachna Chaba, Sueyoung Lee, Krystyna M. Kazmierczak, Karis J. Lee, Angela Wong, Michael Shales, Susan Lovett, Malcolm E. Winkler, Nevan J. Krogan, Athanasios Typas and Carol A. Gross, *Cell* (2011) 144(1), 143156.

[27] Regulation of peptidoglycan synthesis by outer membrane proteins, Athanasios Typas, Manuel Banzhaf, Bart van den Berg van Saparoea, Jolanda Verheul, Jacob Biboy, Robert J. Nichols, Matylda Zietek, Katrin Beilharz, Kai Kannenberg, Moritz von Rechenberg, Eefjan Breukink, Tanneke den Blaauwen, Carol A. Gross and Waldemar Vollmer, *Cell* 2010 143(7), 10971109

[28] Mechanical Behaviour of Bacterial Cell Walls, Thwaites JJ, Mendelson NH., *Adv Microb Physiol.* (1991) 32, 173-222

[29] Peptidoglycan at its peaks: how chromatographic analyses can reveal bacterial cell wall structure and assembly, Samantha M. Desmarais, Miguel A. De Pedro, Felipe Cava and Kerwyn Casey Huang, *Molecular Microbiology* (2013) 89(1), 113

[30] RodZ, a component of the bacterial core morphogenic apparatus, S. Anisah Alyahya, Roger Alexander, Teresa Costa, Adriano O. Henriques, Thierry Emonet and Christine Jacobs-Wagner, PNAS (2009), vol.106, no. 4, 12391244

[31] RodZ, a new player in bacterial cell morphogenesis, Kenn Gerdes, *The EMBO Journal* (2009) 28, 171172

[32] Scott, David W., 1950 Multivariate density estimation: theory, practice, and visualization / David W. Scott p. cm.(Wiley series in probability and mathematical statistics) Includes bibliographical references and indexes. ISBN 0-471-54770-0 (alk. paper) 1. Estimation theory. 2. Multivariate analysis. I. Title. II. Series. QA276.8.S28 1992

[33] Biological Applications of Optical Forces, Karel Svoboda and Steven Block, *Annu. Rev. Biophys. Biomol. Stmct.* (1994).,23:247-85

[34] The bacterial actin MreB rotates, and rotation depends on cell-wall assembly, Sven van Teeffelen, Siyuan Wang, Leon Furchtgott, Kerwyn Casey Huang, Ned S. Wingreen, Joshua W. Shaevitz, and Zemer Gitai, PNAS (2011), vol.108, no.38, 15822-15827

[35] The helical MreB cytoskeleton in E. coli MC1000/pLE7 is an artifact of the N-terminal YFP tag, Matthew T. Swulius and Grant J. Jensen, *J. Bacteriol.* (2012) doi:10.1128/JB.00505-12

[36] The Structure and Function of Bacterial Actin Homologs, Joshua W. Shaevitz and Zemer Gitai, Cold Spring Harb Perspect Biol 2010; doi: 10.1101/cshperspect.a000364

[37] Calibration of optical tweezers with positional detection in the back focal plane, Simon F. Tolic-Nrrelykkea, Erik Schfferb! and Jonathon Howard, Francesco S. Pavone, Frank Jlicher, Henrik Flyvbjerg. *Review of Scientific Instruments* (2006) 77, 103101

[38] Mir M, Babacan SD, Bednarz M, Do MN, Golding I, et al. (2012) Visualizing Escherichia coli Sub-Cellular Structure Using Sparse Deconvolution Spatial Light Interference Tomography. PLoS ONE 7(6): e39816. doi:10.1371/journal.pone.0039816

[39] Cell Wall Nonlinear Elasticity and Growth Dynamics: How Do Bacterial Cells Regulate Pressure and Growth?, Yi Deng Advisor: Joshua W. Shaevitz PhD thesis, Princeton University, USA, November 2012

[40] Mechanisms for maintaining cell shape in rod-shaped Gram-negative bacteria Leon Furchtgott,1 Ned S. Wingreen2 and Kerwyn Casey Huang1 Molecular Microbiology (2011),doi:10.1111/j.1365-2958.2011.07616.x

[41] Combining Modeling and Experiment to Understand Bacterial Growth, Joshua W. Shaevitz, *Biophysical Journal* (2013), vol.104, 2573

[42] Control of Cell Shape in Bacteria: Helical, Actin-like Filaments in Bacillus subtilis, Laura J. F. Jones, Rut Carballido-Lpez and Jeffery Errington, *Cell* (2001), Vol.104, 913922

[43] The molecular origins of chiral growth in walled cells, Kerwyn Casey Huang, David W Ehrhardt and Joshua W Shaevitz, *Current Opinion in Microbiology* (2012) 15,707714

[44] Combining Mathematical Models and Statistical Methods to Understand and Predict the Dynamics of Antibiotic-Sensitive Mutants in a Population of Resistant Bacteria During Experimental Evolution, Leen De Gelder, Jose M. Ponciano, Zaid Abdo, Paul Joyce, Larry J. Forney and Eva M. Top, *Genetics* (2004) 168: 11311144

[45] Motion of variable-length MreB filaments at the bacterial cell membrane influences cell morphology, Christian Reimold, Herve Joel Defeu Soufo, Felix Dempwolff and Peter L. Graumann, *Mol. Biol. Cell* (2013) mbc.E12-10-0728

[46] Theoretical models for the control of bacterial growth rate, abundance, diversity and carbon demand, T. Frede Thingstad and Risto Lignell, *Aquatic Microbial Ecology* (1997), vol.13, 19-27

[47] Dysfunctional MreB inhibits chromosome segregation in Escherichia coli, Thomas Kruse, Jakob Mller-Jensen, Anders Lbner-Olesen and Kenn Gerdes, *The EMBO Journal* (2003), Vol.22 No.19 pp. 5283-5292

[48] MreB, the cell shape-determining bacterial actin homologue, coordinates cell wall morphogenesis in Caulobacter crescentus, Rainer M. Figge, Arun V. Divakaruni and James W. Gober, *Molecular Microbiology* (2004) 51(5), 13211332

[49] Negative Control of Cell Division by mreB, a Gene That Functions in Determining the Rod Shape of Escherichia coli Cells, Masaaki Wachi and Michio Matsuhashi, *JOURNAL OF BACTERIOLOGY* (1989), Vol.171, No.6, 3123-3127

[50]

[51] Determinations of the DNA Sequence of the mreB Gene and of the Gene Products of the mre Region That Function in Formation of the Rod Shape of Escherichia coli Cells, MASAKI DOI, MASAAKI WACHI, FUMITOSHI ISHINO, SHIGEO TOMIOKA, MICHIHIKO ITO, YOUJI SAKAGAMI, AKINORI SUZUKI, AND MICHIO MATSUHASHI, *JOURNAL OF BACTERIOLOGY* (1988), Vol.170, No.10, 4619-4624

[52]

[53] Position-sensitive devices and sensor systems for optical tracking and displacement sensing applications, Anssi Mkynen, Department of Electrical Engineering, University of Oulu, November 3rd 2000

[54] Dependency on Medium and Temperature of Cel Size and Chemical Composition during Balanced Growth of Salmonella typhimurium, M. Schaechter, 0. Maaloe AND N. 0. Kjeldgaard, *J. gen. Microbial.*(1958) 19, 592-606

[55] The A53T mutation is key in defining the differences in the aggregation kinetics of human and mouse -synuclein, Lijuan Kang, Kuen-Phon Wu, Michele Vendruscolo, and Jean Baum *J Am Chem Soc.* (2011) 133(34), 1346513470 doi:10.1021/ja203979j.

[56] Protein structure prediction on the web: a case study using the Phyre server Kelley LA and Sternberg MJE. Nature Protocols 4, 363 - 371 (2009)

[57] Lecture script, 11022-01, Molecular Microbiology, Biozentrum, University of Basel Prof. Guy R. Cornelius, (2010)

[58] Nikolay Ouzounov, Zemer Gitai, LTL, Princeton University, USA

[59] Russel Monde, K.C.Huang, Stanford University, USA

[60] The MreB-Like Protein Mbl of Streptomyces coelicolor A3(2) Depends on MreB for Proper Localization and Contributes to Spore Wall Synthesis Andrea Heichlinger, Moritz Ammelburg, Eva-Maria Kleinschnitz, Annette Latus, Iris Maldener, Klas Flrdh, Wolfgang Wohlleben, and Gnther Muth *Journal of Bacteriology* 2011, vol.193, no.7, 15331542

## Source of Figures

Figure 1: [31]

Figure 2 and 5: pbp-file and homology model [56], graphic: B.Banusch, University of Basel (CH) and Princeton University (USA), 2013

Figure 3: B.Banusch, University of Basel (CH) and Princeton University (USA), 2013

Figure 4: Created by Joshua Shaevitz, Princeton University (USA); re-draw by B.Banusch, University of Basel (CH) and Princeton University (USA), 2013

Figure 6: B.Banusch, University of Basel (CH) and Princeton University (USA), 2013

Figure 7 and 16:Benjamin Bratton, Princeton University (USA) and B.Banusch, University of Basel (CH) and Princeton University (USA), 2013

Figure 8-15,17-18: B.Banusch, University of Basel (CH) and Princeton University (USA), 2013

# 6 Appendix

| Strain | Characteristics | Citation/ source |
|---|---|---|
| SQM259 Rel606 | wild type | R.Monde and KC. Huang [59] |
| SQM260 | mreB-A53T | R.Monde and KC. Huang [55,59] |
| SQM260-14 | mreB-A53T L322Q | R.Monde and KC. Huang [59] |
| SQM260-16 | mreB-A53T G207C | R.Monde and KC. Huang [59] |
| SQM402 | mreB-A53T L209R | R.Monde and KC. Huang [59] |
| Rel 606 | mreB-L322Q | R.Monde and KC. Huang [59] |
| Rel 606 | mreB-G207C | R.Monde and KC. Huang [59] |

Table 4: Bacterial strain description

**Philosophisch-Naturwissenschaftliche Fakultät**
**der Universität Basel**
**Dekanat**

## Erklärung zur wissenschaftlichen Redlichkeit
(beinhaltet Erklärung zu Plagiat und Betrug)

*(bitte ankreuzen)*
☐ Bachelorarbeit
☒ Masterarbeit

Titel der Arbeit *(Druckschrift)*:

Biophysical studies of the effect of MreB mutants on cell stiffness in E.coli

Name, Vorname *(Druckschrift)*: Benjamin Banusch

Matrikelnummer: 07-055-759

Hiermit erkläre ich, dass mir bei der Abfassung dieser Arbeit nur die darin angegebene Hilfe zuteil wurde und dass ich sie nur mit den in der Arbeit angegebenen Hilfsmitteln verfasst habe.

Ich habe sämtliche verwendeten Quellen erwähnt und gemäss anerkannten wissenschaftlichen Regeln zitiert.

Diese Erklärung wird ergänzt durch eine separat abgeschlossene Vereinbarung bezüglich der Veröffentlichung oder öffentlichen Zugänglichkeit dieser Arbeit.

☐ ja ☒ nein

Ort, Datum: Basel, 30.11.2013

Unterschrift:

*Dieses Blatt ist in die Bachelor-, resp. Masterarbeit einzufügen.*